

# Spatial and spectral X-ray properties of the powerful radio galaxy Hercules A: Environment and jet/ICM interaction

J. Siebert<sup>1,2</sup>, N. Kawai<sup>2</sup> and W. Brinkmann<sup>1</sup>

<sup>1</sup> Max-Planck-Institut für extraterrestrische Physik, Giessenbachstrasse, D-85740 Garching, Germany

<sup>2</sup> Institute of Physical and Chemical Research (RIKEN), 2-1 Hirosawa, Wako, Saitama 351-01, Japan

Received 17 May 1999; accepted

**Abstract.** We investigate the X-ray properties of the powerful radio galaxy Hercules A (3C 348) using ROSAT HRI, PSPC and ASCA observations. The ASCA data are well fit by a thermal plasma model with a temperature of about 4.3 keV and abundances 0.4 solar. The HRI observation clearly reveals extended and elongated X-ray emission. For radii greater than 10 arcsec, the surface brightness profile perpendicular to the elongation is well fit by an isothermal  $\beta$ -model with  $\beta = 0.63$  and a core radius of  $\approx 120$  kpc. We derive a total mass of the putative cluster of  $8.4 \times 10^{13} M_{\odot}$  and a gas mass fraction of about 18 per cent. The inner part of the surface brightness profile clearly reveals the presence of a point source, which contributes  $\approx 8$  per cent to the total flux. The 0.1-2.4 keV luminosity of the point-like and the extended emission is  $3.4 \times 10^{43}$  and  $4.3 \times 10^{44}$  erg s<sup>-1</sup>, respectively. After subtracting the cluster X-ray emission from the HRI image, residual structures are visible, which partly coincide with the radio jet and lobes. This indicates an interaction of the radio jet with the intracluster medium.

**Key words:** Galaxies: active; Galaxies: individual – Hercules A; X-rays: general – Radio continuum: galaxies.

## 1. Introduction

The giant elliptical radio galaxy Hercules A (3C 348, 1648+05,  $z = 0.154$ ) is one of the most prominent AGN in the sky with a total radio flux density of 351 Jy at 178 MHz, which makes it the fourth brightest extragalactic radio source. It was one of the first optically identified extragalactic radio sources (Bolton 1948) and has been studied extensively in the radio and optical since then.

A high resolution radio map of Hercules A at 5GHz (Dreher & Feigelson 1984) shows giant radio lobes and prominent jets with spectacular (and still unexplained) ring-like structures. The classification of Hercules A in terms of Fanaroff & Riley (FR) type is ambiguous. Despite its extremely high radio power ( $\log P_{\text{tot},5\text{GHz}} = 27.19$  W/Hz), which is typical for FR II radio galaxies, the radio morphology argues for a FR I classification

(no hot spots visible in the radio lobes, prominent two-sided jets).

Broadband optical imaging revealed two concentrations of light. Thus, Hercules A was originally thought to be a cD galaxy with a foreground star superimposed on it (Greenstein 1962), although already Minkowski (1957) classified it as a double galaxy. Recent photometric work by Sadun & Hayes (1993) supports the idea of a double nucleus with a separation of  $\sim 4''$ , thus indicating merging activity.

The environment of Hercules A has been investigated by several authors (Greenstein 1962, Yates et al. 1989, Allington-Smith et al. 1993), but whether or not Hercules A is associated with a cluster is not yet unambiguously decided. Whereas Yates et al. (1989) claim no particularly rich environment around Hercules A, Allington-Smith et al. (1993) find an excess number of galaxies within 500 kpc of Hercules A. It has to be noted, however, that all studies were based on statistical methods, i.e. number counts, and there is no spectroscopic confirmation of a cluster of galaxies up to now.

In X-rays Hercules A was observed for the first time with the *Einstein* observatory. Dreher & Feigelson (1984) note extended emission on scales of  $\geq$  Mpc and a luminosity of  $3.4 \times 10^{44}$  erg s<sup>-1</sup> in the 0.2–4 keV energy band. However, a detailed analysis of the X-ray data has never been published.

In this paper we present a thorough analysis of the X-ray properties of Hercules A using archival ROSAT data and new ASCA observations. We will show that the X-ray emission is extended and predominantly thermal and that there is interaction between the radio jet and the X-ray emitting gas. The paper is structured as follows: In Sect.2 we analyse the ASCA and ROSAT PSPC data and determine the spectral properties of Hercules A. In Sect.3 we investigate the spatial structure of the X-ray emission using a ROSAT HRI observation and we compare it to the VLA radio map. A discussion of the results is given in Sect.4 and our conclusions are presented in Sect.5. Spatial scales and luminosities are calculated assuming  $H_0 = 50$  km s<sup>-1</sup> Mpc<sup>-1</sup>,  $q_0 = 0.5$  and  $\Lambda = 0$  throughout this paper. At the distance of Hercules A one arcmin corresponds to  $\approx 209$  kpc.

## 2. Spectral analysis

### 2.1. The ASCA and ROSAT PSPC observations

The ASCA observation was performed on August 12 and August 13 1998 in 1-CCD faint mode. The data were analysed using FTOOLS 4.1. The recommended standard screening criteria were applied.

In addition, data taken within 60 seconds after passage of the day-night-terminator and the South Atlantic Anomaly (SAA) were not considered in the analysis. Periods of high background were manually excluded from the data by checking the light curve of the observation. The resulting effective exposures were 35.1 and 34.4 ksec for GIS2 and GIS3 and 33.4 and 32.9 ksec for SIS0 and SIS1, respectively.

Source counts were extracted from a circular region centered on the target with a radius of  $6'$  for the GIS and  $4'$  for the SIS. We used the local background determined from the observation in the analysis for both detectors. In particular, the GIS background was estimated from a source free region at the same off-axis angle as the source and with the same size as the source extraction region. In total,  $\sim 4000$  source photons were detected in each of the SIS detectors.

All spectra were rebinned to have at least 20 photons in each energy channel. This allows the use of the  $\chi^2$  technique to obtain the best fit values for the model spectra. We used the latest GIS redistribution matrices available (V4\_0) from the calibration database and created the SIS response matrices for our observation using SISRMG, which applies the latest charge transfer inefficiency (CTI) table (`sisph2pi_110397.fits`). The ancillary response files for all four detectors were generated using the ASCAARF program.

Spectra were fitted in the energy range 0.8 to 9 keV for both GIS. For SIS0 and SIS1 we used 0.8 to 8 keV. The upper energy boundaries are given by the maximum energy at which the source was detected in each instrument. The lower energy boundaries result from the calibration uncertainties of the detectors. In particular, SIS1 recently shows systematic residuals below 0.6 keV (Dotani et al. 1997). Also, since the CCD temperature of both SIS detectors was rather high during the observation, we decided to ignore all data below 0.8 keV. An increasing RDD (Residual Dark Distribution), which is caused by radiation damage, has been reported for both CCDs. This effect cannot be corrected for with currently available software. However, RDD degradation should be negligible for 1-CCD observations and affects mostly the lowest energy channels, which are excluded from our analysis anyway (Dotani et al. 1997).

The ROSAT PSPC data (ROR 701611) were obtained from the public data archive at MPE. Hercules A was observed with the ROSAT PSPC between August 19 and August 31 1993 with an effective exposure of 8058 sec. The data were prepared for spectral analysis using standard commands within the EXSAS environment. In short, photons were extracted from a circular region with a radius of 5 arcmin centered on the peak of the X-ray emission. The background was determined from a source-free annulus with inner radius 6 arcmin and outer radius 9 arcmin. Only pulse height channels 12 to 240 were used for spectral analysis, because of calibration uncertainties in the

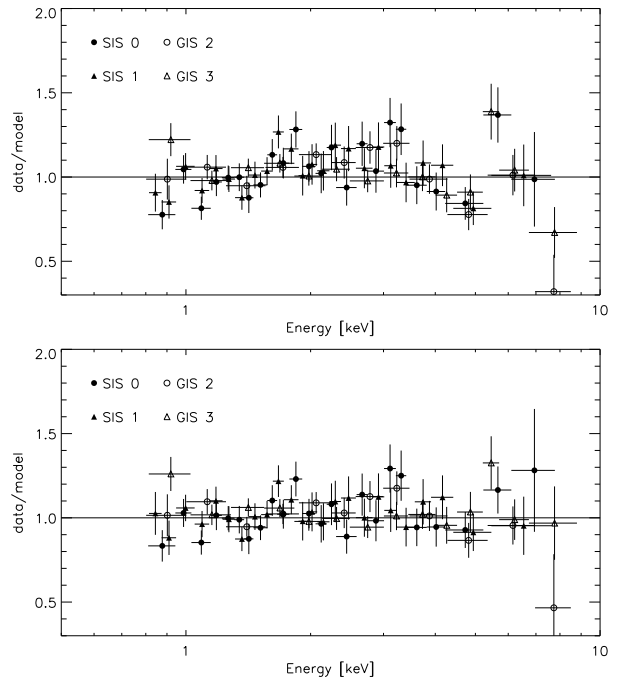


**Fig. 1.** Ratio of the ASCA data from all four detectors to a simple power law model (top panel) and the best-fit thermal model including a five per cent power law contribution from the AGN (bottom panel). The data are rebinned to match the energy resolution of the instruments.

lowest energy channels. The data were rebinned to get a signal-to-noise ratio of at least five in each energy bin. Finally, vignetting and dead time correction were applied to the binned dataset.

### 2.2. Results

We first investigated the data from each detector individually and the results agreed within the errors. In the following we therefore only cite the best-fit model parameters of a simultaneous fit to all four instruments.

The ratio of the ASCA data to a simple power law model with Galactic absorption ( $N_{\text{H}} = 6.40 \times 10^{20} \text{ cm}^{-2}$ ) is shown in the upper panel of Fig. 1. Clearly, there are systematic residuals, in particular above 3 keV. For completeness, we give the best-fit photon index:  $\Gamma = 1.91_{-0.03}^{+0.04}$  ( $\chi^2 = 645.4$  (586 d.o.f.)).

Next we tried a thermal emission model, namely the MEKAL model within XSPEC. The fit improves dramatically ( $\Delta\chi^2 = -61.7$  for one additional parameter). The best-fit parameters are as follows:  $kT = 4.62_{-0.25}^{+0.27}$  keV,  $Z = 0.38 \pm 0.10 Z_{\odot}$  and  $A = (5.0 \pm 0.2) \times 10^{-3} \text{ photons cm}^{-2} \text{ s}^{-1} \text{ keV}^{-1}$ . Since the spatial analysis indicates a small contribution from the central AGN (see Sect.3), we finally included a power law component and fixed its normalization to 10 per cent of the thermal emission. The fit does not further improve ( $\Delta\chi^2 = +1.1$  for one additional parameter), but the model is well consistent with the data ( $\chi_{\text{red}}^2 = 1.00$ ). The best-fit parameters of this model are  $kT = 4.25_{-0.66}^{+1.00}$  keV,  $Z = 0.44 \pm 0.13 Z_{\odot}$ ,

$\Gamma = 1.71_{-0.30}^{+0.74}$  and  $A_{\text{th}} = 4.05_{-0.17}^{+0.14} \times 10^{-3}$  photons  $\text{cm}^{-2} \text{s}^{-1} \text{keV}^{-1}$ . The corresponding data to model ratio is shown in the lower panel of Fig. 1.

If the above model is applied to the PSPC data with all parameters fixed to their best-fit values, we only get a marginally acceptable description of the PSPC spectrum ( $\chi_{\text{red}}^2 = 1.37$  (37 d.o.f.)). However, the fit significantly improves for lower temperatures ( $kT = 2.44_{-0.60}^{+1.33}$  keV; all other parameters fixed to the ASCA values). This might indicate that a single temperature thermal plasma is not a good description for the intracluster medium around Hercules A. In the case of a more complex temperature structure, the relative contribution of the lower temperature plasma in the ROSAT band is higher than in the ASCA band. Therefore the PSPC observation is more sensitive to the lower temperature component, whereas the ASCA measurement is dominated by the higher temperature component. However, the fact that the best-fit temperature determined from the PSPC data is close to the upper end of the PSPC energy range might also indicate that instrumental effects and maybe even residual ROSAT-ASCA cross-calibration uncertainties contribute to the difference in the obtained plasma temperatures from the two instruments.

We further investigated if there is a radial temperature gradient, but found none. Fitting the PSPC data from the inner 45 arcsec and from an annulus with inner radius 45 arcsec and outer radius 3 arcmin separately, we do not find significantly different temperatures ( $kT_{\text{in}} = 2.17_{-0.41}^{+0.83}$  keV compared to  $kT_{\text{out}} = 2.68_{-0.72}^{+1.74}$  keV). Also the (lower resolution) ASCA data do not indicate any temperature gradient.

### 3. Spatial analysis

#### 3.1. The HRI observation

Hercules A was observed with the ROSAT *High resolution Imager* (HRI) between August 28 and September 11 1996 (ROR 702755). The effective exposure of this observation was 21.52 ksec. A second, much shorter (1.2 ksec) observation is not considered in this analysis. The total count rate for Hercules A is  $0.077 \pm 0.010$  cts/s.

Only HRI pulse-height channels 2 to 8 are used in the spatial analysis in order to increase signal-to-noise, as channels 9 to 15 mostly contain instrumental background (cf. David et al. 1997). A contour plot of the total X-ray emission is shown in Fig. 2. The photons were binned in  $2 \times 2$  arcsec pixels and subsequently smoothed with a Gaussian with  $\sigma = 6$  arcsec.

The X-ray emission is clearly extended and elongated. As will be shown later, the direction of the elongation is close to the radio axis of Hercules A. We are confident that the peculiar shape of the X-ray emission is indeed intrinsic and not an instrumental effect, **because** there is a second X-ray source about 4 arcmin to the south-east of Hercules A (R.A. = 16h51m22.3s, Dec = +04d58m23s), which is point-like. It is associated with a stellar object of  $m_V = 12.77$  on the digitized POSS-I plate.

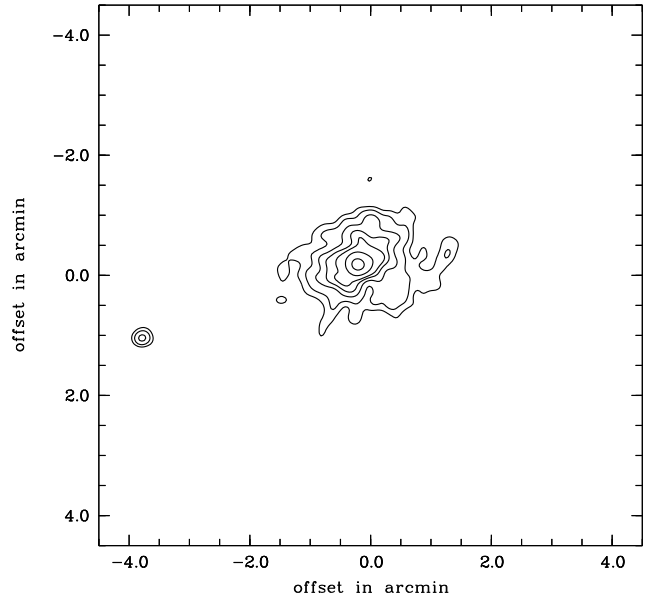


**Fig. 2.** X-ray contours of Hercules A. The contours correspond to 5,8,12,16,20,30 and 50  $\sigma$  above background. The lowest and highest contours denote intensity levels of  $9.4 \times 10^{-3}$  and  $61.8 \times 10^{-3}$  cts  $\text{s}^{-1} \text{arcmin}^{-2}$  respectively.

#### 3.2. Surface brightness profile

To determine the physical properties of the extended X-ray emission we fitted a  $\beta$ -model (e.g. Cavaliere & Fusco-Femiano 1976; Jones & Forman 1984) of the form

$$S(r) = S_0 \left( 1 + \frac{r^2}{r_c^2} \right)^{-3\beta+1/2}$$

to the surface brightness profile of the HRI source. However, we did not use an azimuthally averaged radial profile, but extracted photons from a cone with an opening angle of 90 degrees oriented perpendicular to the elongation of the X-ray emission. Since we intend to subtract the pure cluster emission to see if the residuals are correlated with the radio structure, the above procedure avoids subtracting too much of the extended X-ray emission which originally might be associated with the radio source.

The surface brightness profile, shown in Fig. 3, peaks at the position of the AGN. In the fitting procedure we therefore only used data points for radial distances greater than 10 arcsec to avoid contamination by AGN emission. The best-fit values for the  $\beta$ -model are  $S_0 = 647.1_{-100.5}^{+101.0}$  cts/arcmin<sup>2</sup>,  $\beta = 0.63_{-0.03}^{+0.05}$  and  $r_c = 34.6_{-3.3}^{+3.1}$  arcsec (corresponding to  $120.4_{-11.5}^{+10.8}$  kpc). To account for the central AGN emission we included the Point-Spread-Function (PSF) model (David et al. 1997) for the HRI in the fit. The theoretical PSF-model was convolved with an additional Gaussian ( $\sigma = 1.5$  arcsec) to take into account the known smearing of the PSF by residual wobble motion, which varies between different observations (Morse 1994). For the normalisation of the PSF model we get  $3973.8_{-1090.0}^{+2790.0}$  cts arcmin<sup>-2</sup>. By integrating the two profiles we

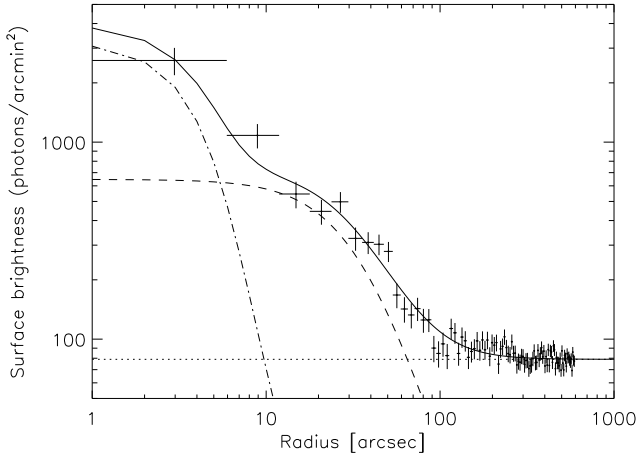


**Fig. 3.** The surface brightness profile for Hercules A. The best-fit  $\beta$ -model is indicated by the long-dashed line, whereas the background level and the PSF model for the central point source are given by the dotted and the dot-dashed lines respectively.

calculate the contribution of the AGN to the total X-ray emission to be about 8 per cent. Assuming a power law spectrum with  $\Gamma = 1.7$  and Galactic absorption we get a 0.1–2.4 keV flux from the point source of  $f_x \approx 3.3 \times 10^{-13} \text{ erg s}^{-1} \text{ cm}^{-2}$  which corresponds to a rest frame 0.1–2.4 luminosity of  $3.4 \times 10^{43} \text{ erg s}^{-1}$ . Hercules A has been noted to be over-luminous in X-rays with respect to its optical continuum and line luminosities (Siebert et al. 1996; Brinkmann et al. 1995). However, these investigations were based on the ROSAT All-Sky Survey data for Hercules A and no separation of extended and AGN emission could be done. The much lower AGN luminosity obtained from our spatial analysis places Hercules A with the bulk of radio galaxies investigated in the above mentioned studies. The flux and luminosity for the extended emission component are  $f_x \approx 4.1 \times 10^{-12} \text{ erg s}^{-1} \text{ cm}^{-2}$  and  $L_x \approx 4.3 \times 10^{44} \text{ erg s}^{-1}$  (assuming a thermal Bremsstrahlung spectrum of  $kT = 4.3 \text{ keV}$ ; see below). The extended X-ray luminosity is typical for clusters of galaxies with Abell richness class two or higher (Ebeling 1993). This would also be consistent with the number counts of Allington-Smith et al. (1993) to determine the galaxy density around Hercules A. In addition, the observed luminosity and temperature for Hercules A are consistent with the well known luminosity-temperature relation for clusters of galaxies (David et al. 1993).

To investigate the residual X-ray emission from the AGN we subtracted the best-fit one dimensional  $\beta$ -model given above from the binned and smoothed HRI image. The resulting X-ray contours overlaid on an optical image from the corresponding POSS-I plate are shown in Fig. 4

The residual X-ray emission is dominated by the point source which is most likely associated with the active nucleus of Hercules A. Several other sources contribute to the remaining X-ray emission. A significant fraction of the diffuse com-

**Fig. 4.** Residual X-ray contours after subtracting the best-fit  $\beta$ -model from the HRI image overlaid on an optical image of the field from the digitized POSS-I plates. The contours correspond to 3,5,8,12,16,24 and 32  $\sigma$  above background. The lowest and highest contour denote intensity levels of  $7.0 \times 10^{-3}$  and  $40.3 \times 10^{-3} \text{ cts s}^{-1} \text{ arcmin}^{-2}$  respectively.

ponent might still be unsubtracted cluster emission, since we assumed a circular symmetry in the cluster subtraction procedure. Part of the emission might also come from additional point sources, for example the bright ( $m_V = 11.97$ ) stellar object to the northwest of Hercules A. Other features, as for example the one-sided jet-like emission and the diffuse component about 1.5 arcmin to the west of Hercules A, correlate with the radio emission. They will be discussed in detail in Sect. 3.4.

### 3.3. Physical parameters of the Cluster emission

By deprojection of the surface brightness profile one can derive the corresponding density profile:

$$n(r) = n_0 \left( 1 + \frac{r^2}{r_c^2} \right)^{-\frac{3\beta}{2}} \quad (1)$$

The central density  $n_0$  is then given by (e.g. Henry et al. 1993):

$$n_0 = 1.2 \times 10^{12} \text{ cm}^{-3} \left[ \frac{I_0}{r_c (kT)^{1/2}} \right]^{1/2} \times \left\{ \frac{\Gamma(3\beta - 1/2)}{\Gamma(3\beta)} \left[ \gamma \left( 0.7, \frac{E_2}{kT} \right) - \gamma \left( 0.7, \frac{E_1}{kT} \right) \right] \right\}^{-1/2}$$

$I_0$  is the central intensity  $S_0$  converted to  $\text{erg cm}^{-2} \text{ s}^{-1} \text{ sr}^{-1}$ ,  $r_c$  the core radius in cm and  $kT$  is given in keV.  $\Gamma$  and  $\gamma$  are the complete and incomplete Gamma functions.  $E_1$  and  $E_2$  denote the observed energy range, i.e. 0.1 and 2.4 keV in our case. For the conversion from  $S_0$  to  $I_0$  we assumed a thermal

bremsstrahlung spectrum with  $kT = 4.3$  keV and Galactic absorption. Using the best-fit parameters from our  $\beta$ -model we obtain  $n_0 = 9.1 \times 10^{-3} \text{ cm}^{-3}$ . By integrating Eq. (1), we can now calculate the total gas mass within a given radius. In the case of Hercules A we get  $1.6 \times 10^{13} M_\odot$  within six times the core radius, i.e. about 600 kpc.

Assuming hydrostatic equilibrium for the intracluster medium of Hercules A and spherical symmetry, we derive the total gravitating mass as a function of radius from the temperature and gas density profiles by applying the hydrostatic equation:

$$M_{\text{tot}}(r) = -\frac{kT_g(r)r}{m_H\mu G} \left( \frac{r}{T_g(r)} \frac{dT_g(r)}{dr} + \frac{r}{\rho(r)} \frac{d\rho(r)}{dr} \right) \quad (2)$$

As discussed in Böhringer et al. (1998), deviations from hydrostatic equilibrium as well as moderate ellipticities do not have a large effect on the mass determination. With the additional assumption of an isothermal intracluster medium, Eq. (2) reduces to

$$M_{\text{tot}}(r) = \frac{3\beta kT_g}{G\mu m_H r_c^2} \frac{r^3}{1 + \frac{r^2}{r_c^2}} \quad (3)$$

For the total gravitating mass within 600 kpc we get  $8.4 \times 10^{13} M_\odot$ . Hence, the gas mass fraction is  $\approx 18$  per cent at this radius.

### 3.4. Radio/X-ray interaction

Fig. 5 shows the radio contours from a 5GHz VLA observation (Dreher & Feigelson 1984), overlaid onto the HRI image after subtraction of the cluster emission according to the best-fit  $\beta$ -model. Several features of the residual X-ray emission coincide spatially with the radio emission: (a) faint knots of X-ray emission are surrounding the outer edges of both radio lobes; (b) there is a bright patch of X-ray emission close to the head of the western radio lobe. It is only slightly displaced from a faint radio feature, which might be interpreted as the head of the advancing radio jet; (c) the orientation of the jet-like feature in the X-ray emission close to the central AGN is aligned with the radio jet; (d) the brightest spot in the eastern radio jet **is bracketed by** enhancements in the X-ray emission. We note that all features are robust in the sense that they also show up when we subtract the cluster emission determined from the azimuthally averaged radial profile.

The close association of X-ray and radio features strongly argues for interaction of the relativistic gas in the radio jet and the thermal gas of the intracluster medium. An X-ray cavity coinciding with the radio lobes has been noted previously for the radio galaxies NGC 1275 (Böhringer et al. 1993) and Cygnus A (Carilli et al. 1994). In the latter case also an enhancement of the X-ray emission close to the edges of the radio lobes was reported. The general physical scenario for these effects (cf. Carilli et al. 1994 **and Clarke et al. 1997 for a more detailed treatment**) is such that the advancing and expanding jet is ploughing its way through the intracluster medium (ICM) thereby expelling the thermal gas from its interior. A

thin sheath of dense, shocked material develops in the vicinity of the advancing head and the expanding tails of the radio lobes. When our line of sight is tangential to the edges of the radio lobes, these density enhancements become visible in X-rays, because thermal X-ray emission is proportional to the square of the gas density. For lines of sight through the center of the radio lobes the X-ray enhancements are probably balanced by an X-ray cavity within the radio lobes due to the expelled gas. The faint patches of X-ray emission surrounding the radio lobes in Hercules A and the bright spot close to the head of the western lobe qualitatively fit into this scenario.

The origin of the jet-like feature in the residual X-ray image is unclear. One might speculate that it is due to synchrotron-self Compton emission from the radio jet. The strength of this ‘X-ray jet’ and the absence of any counter jet would imply that Hercules A is not oriented in the plane of the sky. This obviously is in contradiction to the existence of a double radio jet and the overall symmetry of the radio source (Dreher & Feigelson 1984).

Another interesting feature to note is the close association of the brightest knot in the eastern radio jet and the strongly enhanced X-ray emission to the south (and, at a much lower brightness level, to the north). It almost seems as if the radio jet is squeezed in and probably deflected by local enhancements of the surrounding gas density. But again an unambiguous interpretation is difficult in our case, because the maximum of the X-ray emission is close to a rather bright stellar object on the optical plate, presumably a foreground star, which might contribute significantly to the X-ray flux.

Since X-rays from radio lobes due to inverse Compton scattered cosmic microwave background (CMB) photons are mandatory, we also estimated the amount of X-ray emission expected from this effect. Applying the formalism described in Feigelson et al. (1995), we first determined the magnetic field within the radio lobes from equipartition arguments. As a conservative lower limit we get  $\approx 10\mu\text{G}$ . Using this value for the magnetic field we estimate that at most a flux of  $F_{0.1-2.4\text{keV}} \approx 4 \times 10^{-15} \text{ erg cm}^{-2} \text{ s}^{-1}$  is expected from this process. Since this flux level is about a factor of 20 below the background flux level in our observation, there is no chance to detect these X-rays.

## 4. Summary and conclusions

We investigated the spectral and spatial properties of the X-ray emission of the prominent radio galaxy Hercules A using ROSAT HRI, PSPC, and ASCA observations. The ASCA data clearly favor a thermal plasma model with a temperature of about 4.3 keV and abundances  $\approx 0.4$  solar. A small ( $\approx 8$  per cent) non-thermal contribution of the central AGN is consistent with the ASCA data.

The X-ray source associated with Hercules A is clearly extended in the ROSAT HRI observation. In addition, it is slightly elongated in the direction of the radio jets and lobes. The outer part of the surface brightness profile perpendicular to the radio structure is well described by a King-model with  $\beta = 0.63$  and

**Fig. 5.** Radio contours overlaid onto the HRI image after subtraction of the best-fit  $\beta$ -model. The radio map was obtained with the VLA at 5GHz (Dreher & Feigelson 1984).

a core radius of about 120 kpc. The total mass within 600 kpc is  $8.4 \times 10^{13} M_{\odot}$  and the gas mass fraction is about 18 per cent. A central point source contributing about 8 per cent to the total X-ray flux is clearly needed to fit the surface brightness distribution. We determine a luminosity of  $L_{0.1-2.4\text{keV}} = 3.4 \times 10^{43} \text{ erg s}^{-1}$  for the AGN and  $L_{0.1-2.4\text{keV}} = 4.3 \times 10^{44} \text{ erg s}^{-1}$  for the extended emission.

After subtracting the extended X-ray emission, significant residuals remain in the X-ray image, which partly coincide with the radio emission. They strongly suggest an interaction of the radio jet with the intracluster gas, an effect which has already been noted previously for Cygnus A (Carilli et al. 1994), NGC 1275 (Böhringer et al. 1993) and MRC 0625-536 (Otani et al. 1998).

Spectral and spatial analysis thus provides clear evidence that Hercules A is indeed located in a cluster of galaxies, but spectroscopic observations are needed to unambiguously confirm this interpretation. The non-spherical shape of the extended X-ray emission indicates that the cluster is not relaxed yet, a view which is supported by the identification of a double nucleus in the central cD galaxy, thus indicating an ongoing merging process.

*Acknowledgements.* JS acknowledges financial support from the RIKEN-MPG exchange program. JS also thanks his colleagues from the Cosmic Radiation Laboratory at RIKEN for hospitality and support during a stay at the institute, where part of this work was done. It is a pleasure to thank Eric Feigelson for providing the radio contour map. This research has made use of the NASA/IPAC Extragalactic Data Base (NED), which is operated by the Jet Propulsion Laboratory, California Institute of Technology, under contract with the National Aeronautics and Space Administration.

## References

- Allington-Smith J.R., Ellis R.S., Zirbel E.L., Oemler A. Jr., 1993, ApJ 404, 521
- Böhringer H., Voges W., Fabian A.C., Edge A.C., Neumann D.M., 1993, MNRAS 264, L25
- Böhringer H., Tanaka Y., Mushotzky R.F., Ikebe Y., Hattori M., 1998, A&A 334, 789
- Bolton J.G., 1948, Nat 162, 141
- Brinkmann W., Siebert J., Reich W., et al., 1995, A&AS 109, 147
- Carilli C.L., Perley R.A., Harris D.E., 1994, MNRAS 270, 173
- Cavaliere A., Fusco-Femiano R., 1976, A&A 49, 137
- Clarke D.A., Harris D.E., Carilli C.L., 1997, MNRAS 284, 981
- David L.P., Slyz A., Jones C., et al., 1993, ApJ 412, 479
- David L.P., Harden Jr. F.R., Kearns K.E., et al., 1997, The ROSAT High Resolution Imager (HRI), USRSDC/SAO Calibration Report 1997 June, revised, U.S. ROSAT Science Data Center, SAO, Cambridge, MA
- Dotani T., Yamashita A., Ezuka H., et al., 1997, ASCA News No. 5
- Dreher J.W., Feigelson E.D., 1984, Nat 308, 43
- Ebeling H., 1993, PhD thesis, Universität München
- Feigelson E.D., Laurent-Muehleisen S.A., Kollgaard R.I., Fomalont E.B., 1995, ApJ 449, L149
- Greenstein J.L., 1962, ApJ 135, 679
- Henry J.P., Briel U.G., Nulsen P.E.J., 1993, A&A 271, 413
- Jones C., Forman W., 1984, ApJ 276, 38
- Minkowski R., 1957, IAU Symp. 4, 107
- Morse J.A., 1994, PASP 106, 675
- Otani C., Brinkmann W., Böhringer H., Reid A., Siebert J., 1998, A&A 339, 693
- Sadun A.C., Hayes J.J.E., 1993, PASP 105, 379
- Siebert J., Brinkmann W., Morganti R., et al., 1996, MNRAS 279, 1331
- Yates M.G., Miller L., Peacock J.A., 1989, MNRAS 240, 129

This figure "h1549f4.jpg" is available in "jpg" format from:

<http://arxiv.org/ps/astro-ph/9909450v1>

This figure "h1549f5.gif" is available in "gif" format from:

<http://arxiv.org/ps/astro-ph/9909450v1>